Hindawi
International Journal of Polymer Science
Volume 2024, Article ID 1156880, 14 pages
https://doi.org/10.1155/2024/1156880

Research Article

Silver Nanoparticles Decorated in In Situ Reduced Graphene Oxide Nanohybrids Improved Properties in Poly(vinylidene fluoride)/Poly(methyl methacrylate) Blends

Afifeh Khorramshokouh,[1] Hesam Ramezani,[1] Mehdi Sahami,[1] Mehdi Sharif,[1,2] and Behzad Vaferi[2,3]

[1]*Department of Polymer Engineering, Shiraz Branch, Islamic Azad University, Shiraz, Iran*
[2]*Department of Advanced Calculations, Chemical, Petroleum, and Polymer Engineering Research Center, Shiraz Branch, Islamic Azad University, Shiraz, Iran*
[3]*Department of Chemical Engineering, Shiraz Branch, Islamic Azad University, Shiraz, Iran*

Correspondence should be addressed to Behzad Vaferi; behzad.vaferi@gmail.com

Received 12 December 2023; Revised 21 February 2024; Accepted 7 March 2024; Published 23 March 2024

Academic Editor: Maria Laura Di Lorenzo

In this paper, reduced graphene oxide decorated with silver nanoparticle (rGO-Ag) nanohybrids were prepared using an environmentally friendly approach and incorporated as reinforcement in poly(vinylidene fluoride)-poly(methyl methacrylate) blends via a melt mixing process. The microstructure of rGO-Ag nanohybrids and its effect on the microstructure, mechanical, thermal, and electrical properties of the PVDF/PMM/rGO-Ag was studied using Fourier transform infrared (FTIR), Raman spectroscopy, X-ray diffraction (XRD), scanning electron microscopy (SEM), transmission electron microscopy (TEM), tensile, thermogravimetric analysis (TGA), and impedance spectroscopy methods. FTIR and TEM analysis confirmed that rGO-Ag successfully synthesized and Ag nanoparticles are located on the rGO surface. The tensile analysis demonstrated that incorporating 1 wt.% of rGO-Ag in PVDF/PMMA blend increases Young's modulus and strength of nanocomposite up to 31% and 35%, respectively. The Halpin-Tsai model was also used for PVDF/PMMA/rGO-Ag nanocomposites, and the results confirmed that this model works well to predict the tensile modulus. Impedance spectroscopy analysis showed that the presence of rGO-Ag nanohybrids in PVDF/PMMA blend effectively enhanced the conductivity of PVDF/PMMA blend. TGA results demonstrated that the presence of rGO-Ag nanohybrids enhanced the thermal stability of nanocomposites and increased the degradation temperature of PVDF/PMMA/rGO-Ag nanocomposites in the range of 20°C compared to PVDF/PMMA blend.

1. Introduction

In recent years, the blending of polymeric materials has been a good choice to achieve the requirements in diverse applications [1–4]. The properties of these materials highly depend on the phase morphology [5]. Different methods have been developed to reach the required morphology. Carbon-based fillers such as graphene and its derivatives (e.g., graphene oxide (GO) and reduced graphene oxide (rGO)) have attracted much interest in recent years due to their exceptional properties [6–9]. The incorporation of these fillers with the polymer matrices led to significantly improved properties of nanocomposites [10–13]. rGO is the oxidized form of graphene with relatively lower functional groups than GO which can solve the dispersion problem of graphene sheets [14]. Tajdari et al. observed that fabrication of zinc oxide-titanium dioxide nanohybrid and its dispersion in the poly(lactic acid) matrix gave the best desirable

properties in this polymer compared to single incorporation and simultaneous incorporation [15]. The properties of carbon-based fillers (GO, rGO, carbon nanotube, etc.) can be improved by decorating with other materials [16–20]. Silver nanoparticle is a good choice for improving the properties of polymeric materials [21]. By incorporating them with rGO, new hybrids with desirable properties can be produced. One of the best metal particles for enhancing the properties of rGO is silver nanoparticles (Ag) [22, 23], and the resulting product is known as rGO-Ag nanohybrid. Many studies have used nanohybrids to improve the mechanical properties, thermal stability, electrical conductivity, antibacterial properties, and antifouling properties of nanocomposites [24–26].

PVDF is one of the fluoropolymeric materials with good thermal stability, excellent mechanical properties, resistance to chemical substances, oxidation, and UV irradiation, providing a wide range of applications [27–29]. The main disadvantage of PVDF is its high price; thus, it is often mixed with other polymers to solve this problem [2, 10, 30]. Poly(methyl methacrylate) (PMMA) is a good choice for blending with PVDF to achieve some advantages [31–33]. The miscibility and compatibility of PVDF and PMMA have been extensively studied. They are compatible in a wide range of compositions in solid state, and they are completely miscible in the molten state [34–36]. Their miscibility was achieved from the intermolecular interactions between carbonyl groups of PMMA and the CH_2 and CF_2 groups that existed in PVDF. Researchers observed that blending PVDF with PMMA led to the transfer of crystallization from α phase to β phase, which is thermodynamically unstable in the pure form of PVDF [30, 37, 38]. Polymeric blend nanocomposites made from incorporating PVDF/PMMA blends with nanoparticles also are other materials with enhanced properties [39, 40]. Unique properties of rGO, such as extraordinary mechanical, thermal, and optical properties and good dispersion in polar solvents, make it a good choice to apply as an effective filler for the production of PVDF, PMMA, and PVDF/PMMA blends [41–43]. Liu et al. studied the phase behaviors PVDF/PMMA/GO composites using dynamic rheological measurement. They observed that PMMA chains are anchored on the graphite oxide, and a strong interaction existed between them in the PVDF/PMMA/graphite oxide composites [44]. Sachin et al. prepared PVDF/PMMA/ExGr using the solution blending method and observed that the presence of ExGr increased the crystallization temperature (~4°C) and thermal stability (~11°C) [34]. Sagar et al. investigated the properties of (PMMA)/P(VDF-TrFE)/GO and reported that the value of microhardness and indentation depended on applied load on samples, and the mechanical properties decreased in the presence of GO [35]. Yang et al. studied the structural relaxations of PVDF/PMMA/GO nanocomposites [42]. They observed that the cooperative volume enlarged and dynamic heterogeneity weakened in the presence of GO [42]. Moreover, they found that GO could hinder the crystallization of PVDF but enhanced the miscibility in the PVDF/PMMA amorphous phase [42]. Chiu and Chen produced PVDF/PMMA/Gr and observed that Gr has higher nucleation efficiency for PVDF crystallization and induced PVDF crystals with higher stability [45]. Moreover, they reported that the storage modulus increased by 53.9% (at 25°C) compared with PVDF [45]. Sushmita et al. fabricated two ultrathin multilayered devices using rGO-Fe_3O_4 and MoS_2-Fe_3O_4 nanohybrids that are dispersed in PVDF, mixed with CNT-incorporated PC, and interfacially locked with PMMA [46]. They observed that the storage modulus is as high as 2767 MPa at 40°C (at constant frequency and strain amplitude), and also, the device has high EMI shield effectiveness ((SE_T) of −26.3 dB at 26.5 GHz) [46]. Sushmita et al. investigated the effect of functionalized CNTs on the EMI shielding of PC-based nanocomposites [47]. They observed that CNTs are localized in PC component in PC/PVDF-based blend composites [47]. They also used rGO-Fe_3O_4 nanoparticles to increase thermal conductivity. They found that ball-milled CNTs decreased electrical conductivity compared to pristine CNT-based composites [47]. They reported that the state of filler and its dispersion are the key factors that affected the properties of nanocomposite [47, 48].

To the best of our knowledge, the effect of rGO-Ag nanohybrid dispersion on the microstructure and properties of PVDF/PMMA has not been reported yet. Therefore, in this study, rGO-Ag nanohybrids were synthesized using in situ simultaneous reductions of silver ions in the presence of GO with ascorbic acid as a reducing agent. This process has been done in an aqueous solution, which is a versatile, low-cost, and environmentally friendly process. The rGO-Ag nanohybrids dispersed in PVDF/PMMA blend via melt blending method at different loading ratios and their effect on the morphology and final properties were investigated and discussed.

2. Experimental

2.1. Materials. The materials used were PVDF (solid spot *D* 140, M_w = 20 kg/mol), PMMA (Sigma-Aldrich, M_w = 95 kg/mol), graphite powder (<20 μm, 99.9%), sodium nitrate (Sigma-Aldrich), potassium permanganate (Sigma-Aldrich), sulfuric acid (Sigma-Aldrich), silver nitrate (Sigma-Aldrich, 169 kg/mol), ascorbic acid (Sigma-Aldrich). The GO nanosheets were synthesized using the modified Hummers method according to a previous study [49]. Afterward, GO nanosheets were reduced using ascorbic acid to obtain rGO.

2.2. Green Synthesis of rGO-Ag Nanohybrids. In order to prepare rGO-Ag nanohybrids, 0.8 g of GO powder was dispersed in 40 ml distilled water using ultrasonication for 1 h. Then, the stabilized GO colloid was transferred to a 500 ml flask containing a solution of distilled water and silver nitrate (4 g $AgNO_3$ in 40 ml distilled water), and 1.76 ml of ascorbic acid, which was dissolved in 30 ml distilled water, was gradually added to the solution to extract Ag ions from $AgNO_3$ and reduce oxygen-containing groups of GO. The mixture was then stirred for 2 h. Finally, rGO-Ag nanohybrids were separated from the solution and dried in a vacuum oven for 24 h at 85°C. For comparison, the above process was done without adding $AgNO_3$ to prepare rGO.

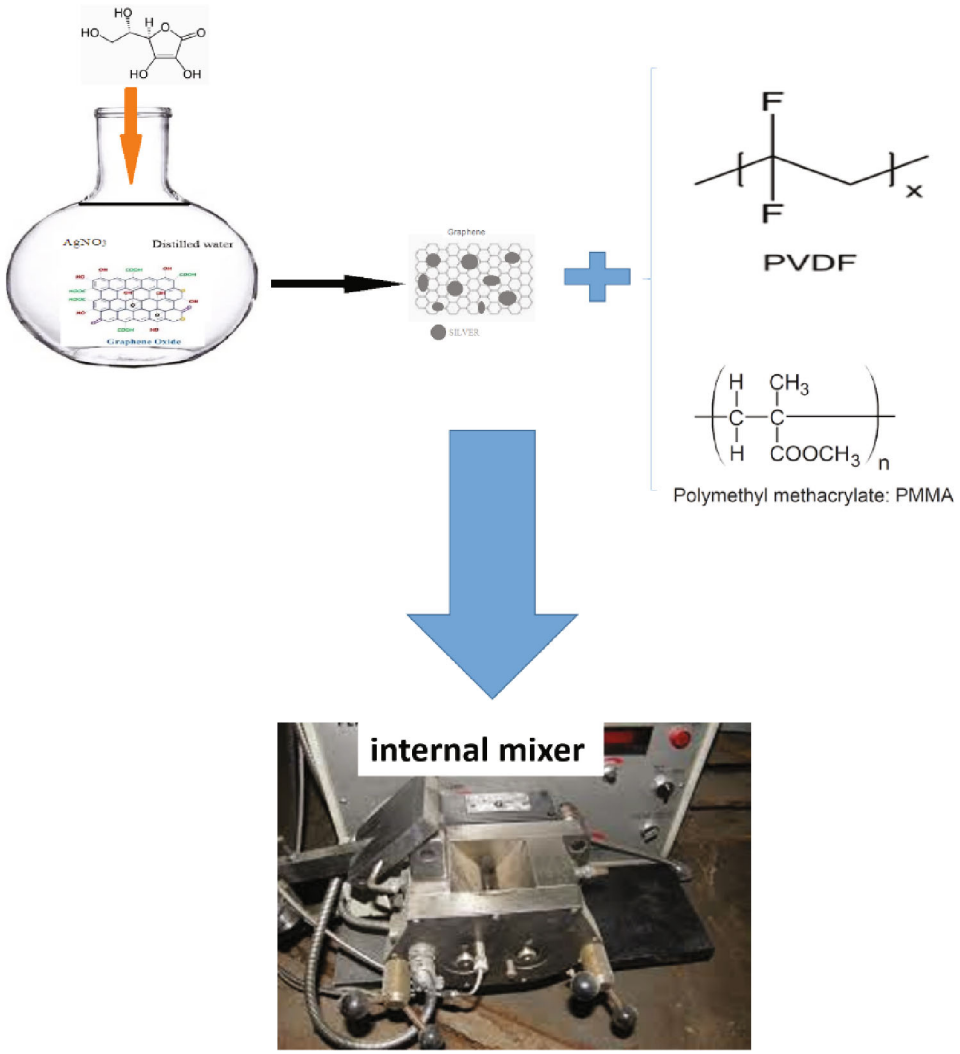

Figure 1: Schematic of rGO-Ag-filled PVDF/PMMA nanocomposite preparation.

2.3. Preparation of the PVDF/PMMA/rGO-Ag Nanocomposites. Polymer nanocomposites were prepared by melt mixing method. For this purpose, rGO-Ag nanoparticles were mixed with PMMA/PVDF blends using an internal mixer at 180°C and 60 rpm as illustrated in Figure 1. The concentration and nomenclature of each component are presented in Table 1.

2.4. Characterization. X-ray diffraction measurements were measured with a WAXD diffractometer (D8 Advance, Bruker, USA). X-ray patterns of samples were obtained via Cu-Ka radiation ($\lambda = 0.15406$ nm, 40 kV, and 30 mA) in the range of 2θ angle of 5° to 70° at the scan rate of 1°/min and step size of 0.1°.

FTIR spectra were carried out using a FTIR spectrometer (1600, Perkin-Elmer Co., MA) from 4000 to 400 cm^{-1}. Approximately 0.1 to 1.0% sample is well mixed into 200 to 250 mg of potassium bromide (KBr) powder, and then, a force of approximately 8 tons is applied under a vacuum of several mm Hg for several minutes to form transparent pellets.

Raman spectra were recorded between 750 and 3000 cm^{-1} by a Nanofinder 30 confocal Raman microscope (Senterra,

Table 1: Composition and codes of the prepared samples.

Sample	Composition (%)		
	PVDF	PMMA	GO-Ag
PVDF	100	0	0
PV 0.8	80	20	0
PV 0.7	70	30	0
PV 0.6	60	40	0
PV/PM	50	50	0
PM 0.6	40	60	0
PM 0.7	30	70	0
PM 0.8	20	80	0
PMMA	0	100	0
PM 0.8/rGO-Ag 0.5	20	80	0.5
PM 0.8/rGO-Ag 1	20	80	1
PM 0.8/rGO-Ag 1.5	20	80	1.5

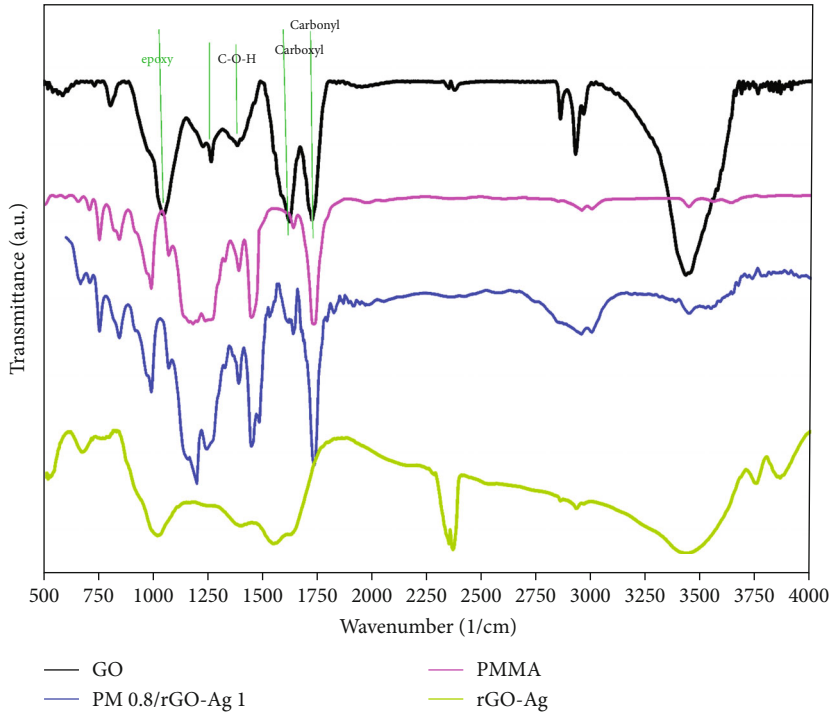

Figure 2: FTIR diffraction of rGO-Ag nanohybrids, GO, and nanocomposites.

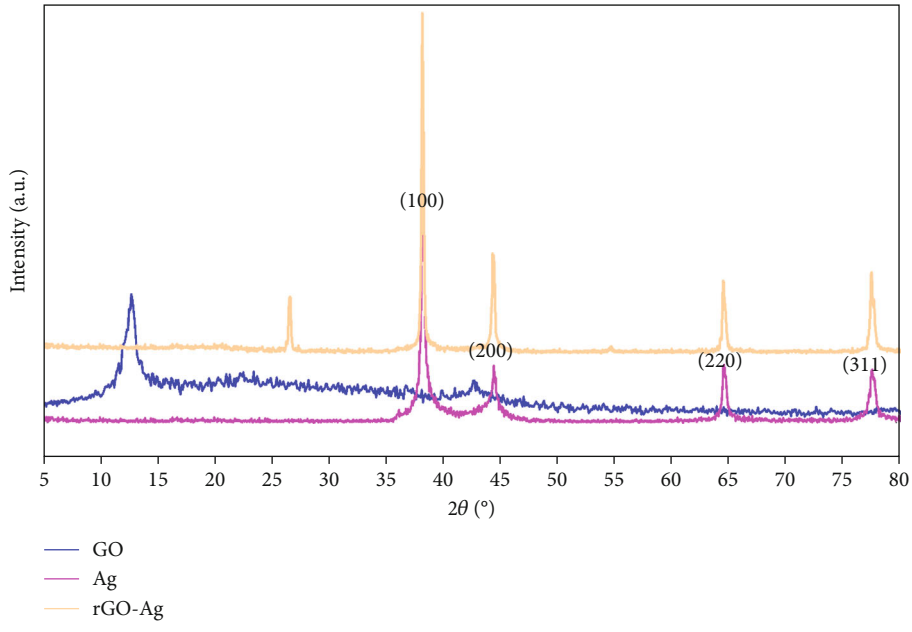

Figure 3: X-ray diffraction of GO nanosheets in comparison with rGO-Ag nanosheets.

Bruker) equipped with a CCD detector and at 785 nm of laser excitation.

The electrical properties of samples were measured using a D8 Advance machine at a frequency rate of 20-20000 Hz.

Scanning electron microscopy (SEM; JEOL-6700F) was used to investigate the microstructure of rGO-Ag and its dispersion in chitosan matrix. For this propose, the fracture surfaces of filler and fractured surface of samples were obtained after the tensile analysis was covered via a thin layer of goal and observed at 5 kV.

The TEM analysis of rGO-Ag was performed by the JEOL 2100 instrument. A small amount of the sample was dispersed in acetone through sonication, and a drop of this dispersed solution was put on the copper grid for HRTEM analysis.

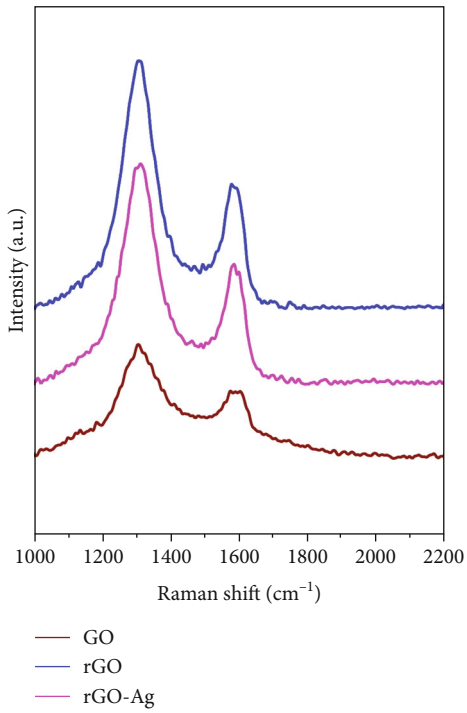

Figure 4: Raman spectra of the GO, rGO, and rGO-Ag nanocomposite.

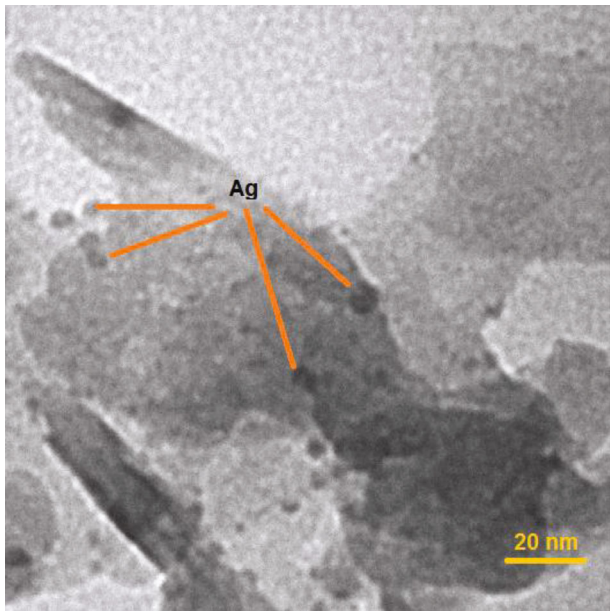

Figure 5: TEM images of rGO-Ag nanohybrids.

The mechanical properties of the films were measured on a universal tensile tester (ASTM-D360 Instron 4301, Instron, USA) at a speed of 1.2 mm/min according to ISO527-3-1995 (E). Five samples of each formulation were tested, and averages of Young's modulus (E), ultimate tensile strength, and elongation at break were evaluated from stress-strain curves.

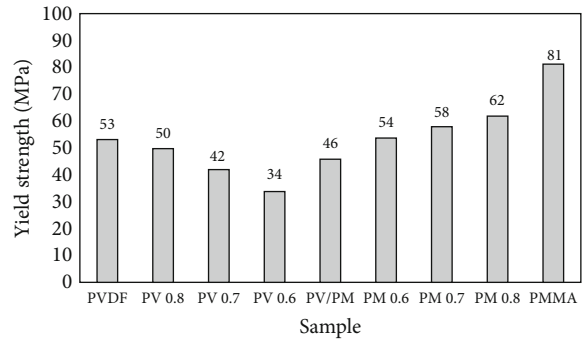

Figure 6: Yield strength of PVDF, PMMA, and PVDF/PMMA blends.

Thermogravimetric analysis (TGA) was carried out by TA Instruments SDT Q600 to investigate the thermal properties of the samples. The test was carried out under a nitrogen atmosphere and a heating rate of 10°C per minute in the temperature range of 25-700°C.

The dielectric permittivity was measured by a LCR meter (Agilent, E4980A) equipped with a dielectric test fixture (Agilent, 16451B) in the frequency range of 100 to 10000 kHz. The samples used for the tests were disc pellets with a diameter of 5 mm, and the average thickness was about 0.5 mm. A piece of rectangular standard Teflon sample with a permittivity of 2.1–2.4 was used for calibration before each test.

3. Results and Discussion

3.1. Characterization of GO Nanosheets and rGO-Ag Nanohybrids

3.1.1. FTIR Spectroscopy. Figure 2 represents the FTIR spectroscopy of GO, rGO-Ag nanohybrids, and nanocomposites. In this figure, the peaks at 1720, 1618, 1400, 1260, 1132, and 1049 cm^{-1} wavenumber of GO are related to the carbonyl and carboxyl groups, C-O-H functionality, breathing vibrations of epoxide group, and C-O stretching vibrations of GO [14].

For rGO-Ag nanohybrids, the peaks are very similar to GO nanosheets. However, the intensity of these peaks may be reduced due to the reduction of GO nanosheets with ascorbic acid in the presence of Ag [25, 50, 51]. In the spectrum of rGO-Ag, the band at 1049 cm^{-1} (related to C-O group) broadened and shifted to a higher frequency due to the reduction of graphene sheets. Moreover, the peak in 1387 cm^{-1} associated with the in-place deformation of O-H bonds in hydroxyl groups of GO disappeared in FTIR spectra of rGO-Ag due to the reduction of GO with ascorbic acid [31]. The chemical structure of rGO-Ag-filled nanocomposites was also studied using FTIR analysis. In this figure, the absorption in the region of 2998, 2955, and 1387 cm^{-1} was attributed to the stretching vibration of C-H in methylene and methyl groups of PMMA [45]. Moreover, the peak appeared at 1727 cm^{-1} was related to the carbonyl stretching and characteristic peak at 200 and 1148 cm^{-1} attributed to

C-O stretching. From the FTIR analysis, it can be concluded that the intensity of the carbonyl stretching frequency in the PMMA/rGO-Ag nanocomposites is higher than that one in pure GO and PMMA. This may be due to the polar-polar interaction between the methacrylate (-$COOCH_3$) group of PMMA and carbonyl functionality of rGO-Ag.

3.1.2. XRD. The XRD patterns of GO nanosheets, Ag, and rGO-Ag nanohybrids are presented in Figure 3. In the XRD pattern of GO, the peak at $2\theta = 10.13^\circ$ was observed. When the graphite was oxidized to form GO, the GO exhibited a broad diffraction peak at $2\theta = 10.13^\circ$, corresponding to an interlayer spacing of 0.842 nm. Large interlayer distances have been attributed to the formation of hydroxyl, epoxy, and carboxyl groups [52]. The main peak in the XRD pattern of GO at $2\theta = 10.13^\circ$ disappeared in the XRD pattern of rGO-Ag nanohybrids. This evidence suggested that the GO was fully transformed into rGO by the reduction of oxygen-containing functional groups, and this indicates that ascorbic acid has reduced oxygen-containing groups of GO nanosheets to a great extent [53]. Apart from that, the higher intensity of the characteristic peaks related to the Ag part of the nanohybrids compared with GO implies that Ag nanoparticles facilitated the exfoliation of rGO nanosheets leading to the disappearance of the peak at $2\theta = 10.13^\circ$ [25].

The XRD profile of Ag has four peaks at $2\theta = 38.3^\circ$, 44.4°, 64.6°, and 77.4°, which correspond to the (111), (200), (220), and (311) crystallographic planes, respectively [31]. The XRD pattern of rGO-Ag has a characteristic peak of Ag and also a peak at 24° due to the reduction of GO and Gr preparation. The Ag peaks in the XRD profile of Ag-GO were observed due to the presence of silver nanoparticles on the surface of rGO nanosheets. The average crystalline size D of the silver nanoparticle have been estimated from the diffractogram by using the Debye-Scherrer formula, $D = 0.9\lambda/\beta \cos\theta$, where λ is the wavelength of the X-rays used for diffraction and β is the full width at half maximum (FWHM) of a peak [54]. The average crystalline size of the silver nanoparticles is found to be 30 nm. The value of the interplanar spacing between the atoms, d, has been calculated using Bragg's law, $2d\sin\theta = n\lambda$, where n is the order of diffraction pattern. In the present case, n is equal to 1. From the four datasets for the four peaks, four values of d are obtained and four values are nearly the same (1.5 A°~2 A°).

3.1.3. Raman Spectroscopy. Figure 4 shows Raman spectra of GO, rGO, and rGO-Ag composite. GO peaks at 1325 cm^{-1} and 1580 cm^{-1} correspond to D band and G band. In rGO, the D band and G band are observed at 1319 cm^{-1} and 1585 cm^{-1}, which are shifted in rGO-Ag to 1310 cm^{-1} and 1572 cm^{-1}. The ratio of the intensity of D/G in GO was found around 1.66, while in rGO, it increases to 1.99, but in rGO-Ag, it is 1.8. The increase in D/G ratio indicates that there is a decrease in the average size of sp^2 carbon domain after the synthesis of rGO and rGO-Ag from GO [55, 56].

3.1.4. TEM Images. The TEM image of rGO-Ag nanohybrid is presented in Figure 5. As shown in this figure, the

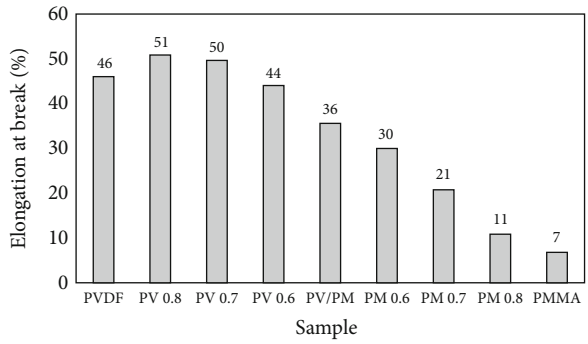

Figure 7: Elongation at break of PVDF, PMMA, and PVDF/PMMA blends.

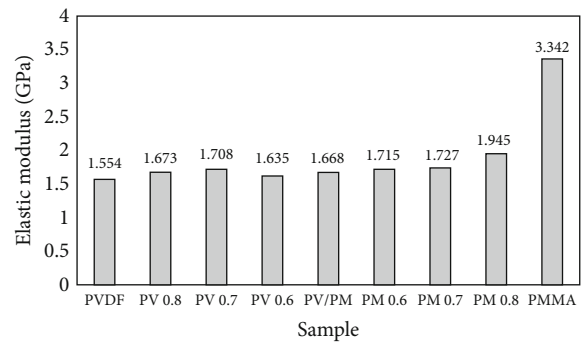

Figure 8: Elastic modulus of PVDF, PMMA, and PVDF/PMMA blends.

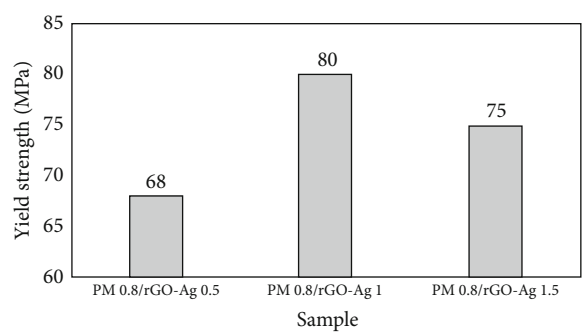

Figure 9: Yield strength of the nanocomposites.

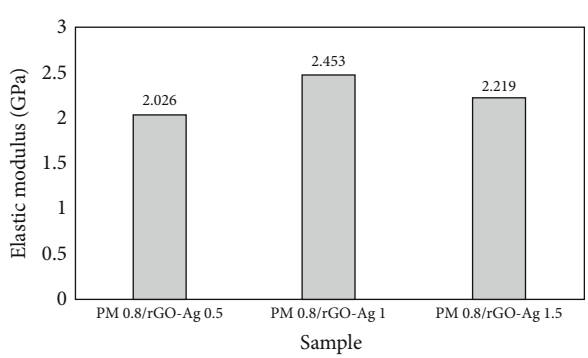

Figure 10: Elastic modulus of the nanocomposites.

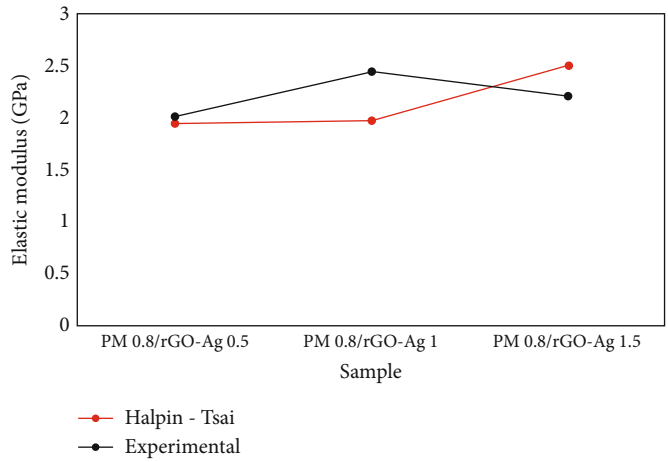

Figure 11: Comparison between the elastic modulus calculated by the Halpin-Tsai equation and experimental data.

crumpled and wrinkled surface of rGO is stacked together to form a multilayer structure that embraces the Ag nanoparticles and modifies their surface energy which is the main reason for the agglomeration Ag nanoparticles. Furthermore, because of the different extent of reduction in various rGO nanosheets, Ag nanoparticles have to compete with each other to attach to the surface of rGO nanosheets which have more oxygen-containing groups on their surface. This means that those nanosheets which had been reduced more can interact with fewer Ag^+ ions because of the limited OH^- ions available on their surface. Hence, Ag^+ ions tend to interact with nanosheets with more OH^- ions available [57].

3.1.5. Mechanical Properties of PVDF/PMMA Blends. Mechanical properties are the most important factor when it comes to application, and many polymers are being chosen to be used in different applications because of their superior mechanical properties. Thus, to find out the best blend composition to be reinforced with the nanohybrids, the mechanical properties of every sample were measured and compared together in Figures 6–8. Samples with PVDF as their matrix showed a downtrend in yield strength as the PMMA content increased up to 40 wt.%; after this turning point, yield strength is directly related to the PMMA content because it is the new matrix and has better mechanical properties than PVDF. According to Figure 5, PM 0.8 sample has the highest yield strength (62 MPa) due to the superior mechanical properties of PMMA and the possible changes in the crystalline structure of the samples [58]. As for the elongation at break, results showed that by increasing the PMMA content, the elongation at break of the samples decreases because of the nature of PMMA which has a low tensile strain. It can be observed that for the PV 0.8 sample, elongation at break increases which can be due to the addition of PMMA and the lower crystallinity and formation of the β crystalline phase in PVDF, but this trend changes as soon as the PMMA content starts to rise [59]. At this point, the mechanical properties of the blend will be attributed to the high strength and the low tensile strain of the glassy phase. It is to be noted that the strong interactions between PVDF and PMMA chains lead to the enhancement of mechanical properties of the nanocomposites [60, 61].

Elastic modulus does not follow a specific trend, and it varies with the composition. However, as PMMA becomes the dominant phase, a certain uptrend can be recognized, which climaxes at 1.945 GPa for PM 0.8. Once again, this increase results from the superior mechanical properties of PMMA which has a high elastic modulus compared to PVDF.

Finally, results showed that PM 0.8 possesses the best mechanical properties and the potential to be used in applications that require desirable yield strength and elastic modulus. Consequently, PM 0.8 was chosen to be reinforced with 0.5, 1, and 1.5 wt.% of rGO-Ag nanohybrids.

3.2. Characterization of PVDF/PMMA/rGO-Ag Nanocomposites

3.2.1. Mechanical Properties. Tensile strength, elongation at break, and elastic modulus of the PM 0.8/rGO-Ag 0.5, PM 0.8/rGO-Ag 1, and PM 0.8/rGO-Ag 1.5 are presented in Figures 9 and 10. It can be observed that tensile strength and elastic modulus experienced an improvement with the increase of rGO-Ag nanohybrids, while elongation at the break of the samples decreased. In addition to that, PM 0.8/rGO-Ag 1 sample has shown the highest yield strength and elastic modulus compared to other nanocomposites with 80 MPa and 2.453 GPa, respectively. As the PM 0.8/rGO-Ag 1.5 sample has a superior yield strength and elastic modulus to PM 0.8 and PM 0.8/rGO-Ag 0.5 samples, it can still not compete with PM 0.8/rGO-Ag 1, which can be mainly due to the agglomeration of the nanohybrids inside the polymer matrix. The improved dispersion state observed in hybrid nanocomposites can be attributed to two plausible explanations. The first explanation suggests that multilayer platelet-shaped nanofillers can function as bridges between spherical/cylindrical nanofillers, thereby preventing their reaggregation. The second explanation proposes that spherical/cylindrical nanofillers can hinder the restacking or reaggregation of exfoliated platelet-shaped nanofillers, leading to enhanced dispersion [62–64]. Silver nanoparticles have a high tendency to form agglomerates inside many polymer matrices to minimize their surface energy. Hence, rGO

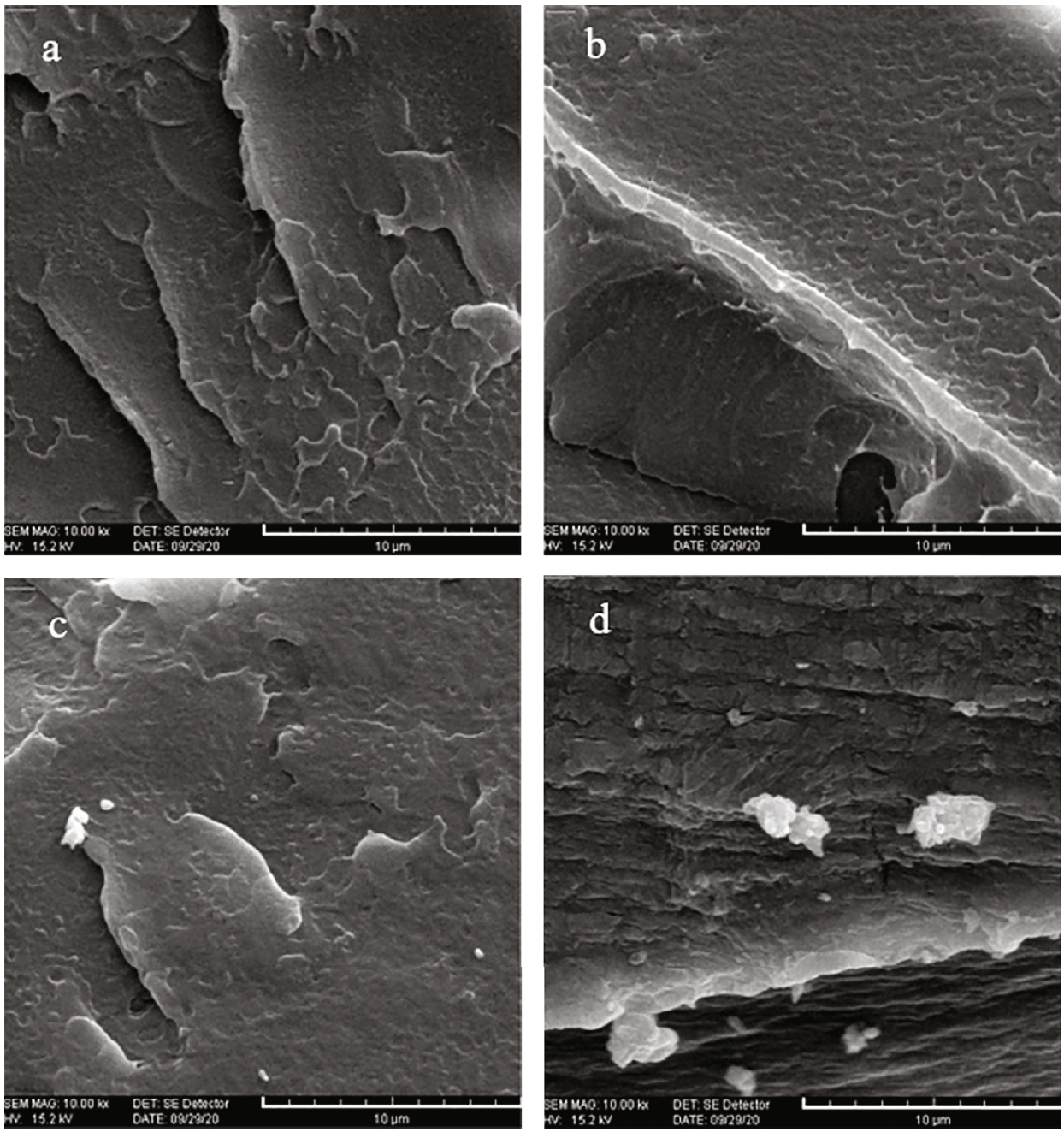

Figure 12: SEM images of (a) PM 0.8, (b) PM 0.8/rGO-Ag 0.5, (c) PM 0.8/rGO-Ag 1, and (d) PM 0.8/rGO-Ag 1.5.

nanosheets are used to hold these nanoparticles in place and prevent them from forming agglomerates. By adding 1.5 wt.% of the nanohybrids and increasing the silver content inside the matrix, it can be presumed that silver particles had the chance to form agglomerates and negatively impact the mechanical properties of the nanocomposite [50, 65–69].

3.2.2. Halpin-Tsai Model. One of the most widely used models for predicting elastic modulus in composites consisting of two phases is the Halpin-Tsai model. Since it can be presumed that the PVDF/PMMA part of the composites acts as an integrated matrix and rGO-Ag nanohybrids disperse inside them, then the Halpin-Tsai model can be used for the prediction of elastic modulus. This model can also help determine the morphology of the matrix and the efficiency of filler dispersion. The Halpin-Tsai model is given by Equation (1), which was also used in similar calculations by other researchers to predict the properties of binary composites.

$$\frac{E_1}{E} = \frac{(1 + A_i B_i \varphi_2)}{(1 - B_i \varphi_2)}. \quad (1)$$

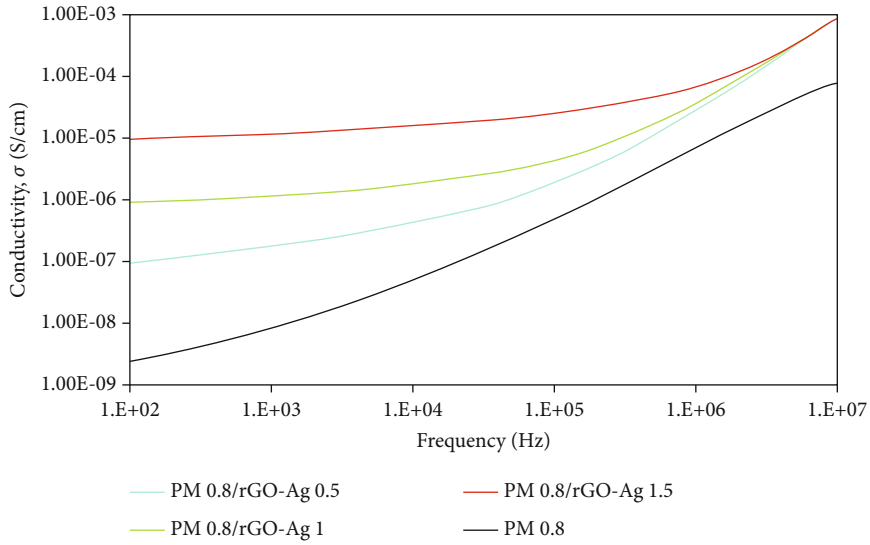

Figure 13: The conductivity of PM 0.8 and the nanocomposite samples.

B_i can be calculated using the following:

$$B_i = \frac{(E_1/E_2) - 1}{(E_1/E_2) + A_i}. \quad (2)$$

Subscripts 1 and 2 represent the matrix and the dispersed phases, respectively, and φ_2 shows the filler volume fraction. As for the constant A_i, it can be determined with respect to the morphological properties of the system. For the dispersed phase consisting of hard materials such as rGO-Ag nanohybrids, A_i equals to 1.5. E_1 and E_2 should also be determined to use the equations, which are the elastic modulus of PM 0.8 and rGO-Ag nanohybrids, respectively. According to Figure 8, the elastic modulus of PM 0.8 is 1.945 GPa, but for the nanohybrids, it was presumed that silver nanoparticles are not able to further increase the modulus of rGO. In addition, they act as conductive interfaces between rGO and the matrix, which presumably transfer the loads to their substrate, in other words, rGO. Hence, E_2 was presumed to be the theoretical value for the elastic modulus of rGO, which is approximately 325 GPa. The results of the Halpin-Tsai calculations are presented and compared with experimental elastic modulus values in Figure 11.

As shown in the figure, there is a certain inconsistency between the obtained values from the equation and the experimental data. The reason for the observed difference in PM 0.8/rGO-Ag 1.5 can be related to the fact that the Halpin-Tsai equation does not take the agglomeration of the fillers into account; as a result, it predicts that the modulus should continue to rise with the addition of fillers. However, fillers with planar geometry tend to agglomerate in relatively low concentrations, which has also happened for samples containing 1.5 wt.% of the nanohybrids. The reason for the inconsistency between the results for PM 0.8/rGO-Ag 1 can be attributed to the synergistic effect of the good dispersion of the nanohybrids and the interactions between nanohybrids and the matrix.

3.2.3. Morphological Observation. The SEM analysis was used to investigate the effect of rGO-Ag on the morphology of PMMA/PVDF blends, and the results are presented in Figure 12. It can be seen that the two amorphous and semicrystalline phases of PMMA and PVDF are compatible with each other, and they have formed a homogenous system (Figure 12(a)). Figure 12(b) shows that in PM 0.8/rGO-Ag 0.5 nanocomposites, the rGO-Ag nanohybrids have a good dispersion, and no agglomerates are observed. But with an increase in the rGO-Ag content (PM 0.8/rGO-Ag 1), the agglomeration of filler was observed (Figure 12(c)) due to the effective interactions between oxygen-containing functional groups on the rGO and CF_2 segments in PVDF and also the strong interactions between the rGO nanosheets [37, 70]. Figure 12(d) also shows that agglomerations occurred at its fracture surface, leading to a decrease in load transfer between the matrix and filler and reduced mechanical properties.

3.2.4. Impedance Spectroscopy. Figure 13 compares the conductivity of the PVDF/PMMA blend and PMMA/PVDF/rGO-Ag nanocomposites as a function of frequency. From this figure, it can be seen that the conductivity of PVDF/PMMA increased linearly with the increase in frequency. But for rGO-Ag-filled PVDF/PMMA nanocomposites (0.5, 1, and 1.5 wt.%), the conductivity is almost independent of the frequency change in the low-frequency range. In fact, when the volume fraction of conductive filler is less than the percolation threshold, the conductivity increases almost linearly with the increase of frequency; but when the volume fraction of conductive filler is higher than the percolation threshold, the conductivity values are much greater leading the conductivity to be almost independent of frequency [71, 72]. The results show that due to the synergistic effect between the electrical properties of silver particles and

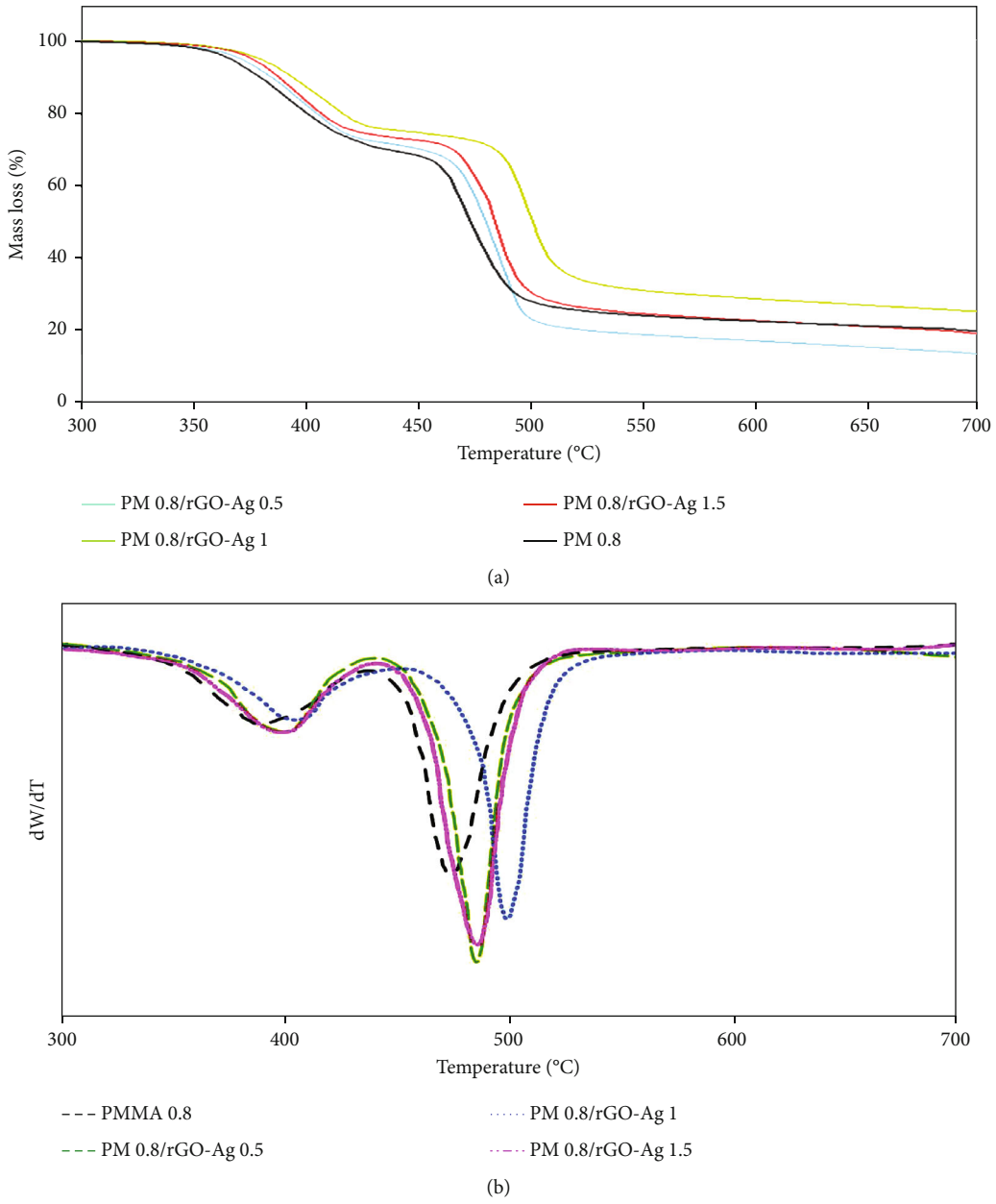

Figure 14: Thermogravimetric analysis of PM 0.8 and nanocomposite samples.

rGO, the electrical conductivity of PMMA/PVDF blends enhanced [73].

3.2.5. Thermogravimetric Analysis. Thermal behavior and stability of PM 0.8 and nanocomposite samples were determined using thermogravimetric analysis, and test results are shown in Figures 14(a) and 14(b). As shown in the figure, the general thermal profiles of all the samples are quite the same and consist of two stages. These stages are related to the degradation of PVDF and PMMA contents of the samples. With the introduction of rGO-Ag nanohybrids, both degradation stages occur at higher temperatures which can be attributed to the thermal stability of Ag nanoparticles and rGO nanosheets. The PM 0.8/rGO-Ag sample has the highest thermal stability and the lowest degradation related to the better dispersion of nanohybrids inside the nanocomposite and higher density of interactions between the matrix and nanohybrids [45, 53]. The PMMA portion of the samples started to degrade at around 360°C for PM 0.8 sample and increased to a maximum of 375°C for the PM 0.8/rGO-Ag 1 nanocomposite. Apart from that, the PVDF part of the samples started the thermal degradation at 462°C for the PM 0.8 sample and reached 480°C for PM 0.8/rGO-Ag 1 nanocomposite. These observations can result from retarding the chain scission of C-F and C-H bonds of the PVDF by providing a thermal shield by the nanohybrids and trapping the free radicals produced in the system. Thus, thermal stability and degradation temperature increase with the addition of nanohybrids into the system [45, 74]. The enhanced thermal properties of rGO-Ag-filled PVDF/

PMMA nanocomposites compared with PM 0.8 sample might be attributed to one of the following: (a) this suggests that rGO-Ag acts as a barrier to hinder the volatile decomposition products throughout the composites. (b) The Ag content on rGO in the PM 0.8 matrix brought the well dispersion. Moreover, the degradation of rGO-Ag-containing groups degrades and forms heat-resistant residues, which increased char residues. The thermal stable char residues limited the production of combustible gases and the diffusion of heat, resulting in the improved thermal stability of PM 0.8 composites.

4. Conclusion

Reduced graphene oxide decorated with silver nanoparticle (rGO-Ag) nanohybrids were prepared using an environmentally friendly approach and incorporated in poly(vinylidene fluoride)-poly (methyl methacrylate) blends via the melt mixing process to study their effect on the structure and properties of the blends. The mechanical, thermal, and electrical properties of the PVDF/PMM/rGO-Ag were analyzed using FTIR, Raman spectroscopy, XRD, SEM, TEM, tensile, TGA, and impedance spectroscopy methods. Results demonstrated that by adding even a low content of the nanohybrids to the blends, the resulting nanocomposites show better mechanical, thermal (conductivity, thermal stability, and the degradation temperature), and electrical properties than the PVDF/PMM blend. These improved properties demonstrate that rGO-Ag nanohybrids can be considered reinforcing fillers to add different properties to PVDF/PMMA blends to facilitate their usage in various applications. Also, the tensile modulus of PVDF/PMMA/rGO-Ag nanocomposites is simulated using the Halpin-Tsai model.

Data Availability

The datasets used and/or analyzed during the current study are available from the corresponding author on reasonable request.

Disclosure

A preprint has previously been published [75].

Conflicts of Interest

The authors declare that they have no known competing financial interests or personal relationships that could have appeared to influence the work reported in this paper.

Authors' Contributions

Material preparation, data collection, and analysis were performed by Afifeh Khorramshokouh, Hesam Ramezani, Mehdi Sahami, and Mehdi Sharif. The first draft of the manuscript was written by Afifeh Khorramshokouh, and all authors commented on previous versions of the manuscript. The last author (Behzad Vaferi) checked the results and reviewed the final manuscript. All authors read and approved the final manuscript and agreed to publish the results.

References

[1] T. Hosoda and T. Yamada, "Effect of TiO_2 on morphology and mechanical properties of PVDF/PMMA blend films prepared by melt casting process," *Journal of Applied Polymer Science*, vol. 131, no. 13, 2014.

[2] H. Ramezani, M. Sharif, and A. K. Shokooh, "Graphene-based polymer nanocomposites," *Basparesh*, vol. 4, no. 4, pp. 86–107, 2015.

[3] A. Ehsani, A. A. Heidari, H. Mahdavi, M. Bigdeloo, and M. Kalhor, "Enhanced electrochemical performance of redox conductive polymer in the presence of high efficient modified reduced graphene oxide," *Applied Nanoscience*, vol. 11, no. 9, pp. 2459–2467, 2021.

[4] M. Hernández-López, Z. N. Correa-Pacheco, S. Bautista-Baños et al., "Bio-based composite fibers from pine essential oil and PLA/PBAT polymer blend," *Morphological, physicochemical, thermal and mechanical characterization, Materials Chemistry and Physics*, vol. 234, pp. 345–353, 2019.

[5] J. Wang, M. A. Ayari, A. Khandakar et al., "Estimating the relative crystallinity of biodegradable polylactic acid and polyglycolide polymer composites by machine learning methodologies," *Polymers*, vol. 14, no. 3, p. 527, 2022.

[6] M. Pandey and M. Balachandran, "Flexible polymer composite films incorporated with Li-ion/reduced graphene oxide: excellent optical and photoluminescence performance," *Applied Nanoscience*, vol. 10, no. 2, pp. 401–410, 2020.

[7] M. N. Muralidharan, S. Mathew, A. Seema, P. Radhakrishnan, and T. Kurian, "Optical limiting properties of in situ reduced graphene oxide/polymer nanocomposites," *Materials Chemistry and Physics*, vol. 171, pp. 367–373, 2016.

[8] A. Shafiq, A. B. Çolak, and T. N. Sindhu, "Significance of EMHD graphene oxide (GO) water ethylene glycol nanofluid flow in a Darcy–Forchheimer medium by machine learning algorithm," *European Physical Journal Plus*, vol. 138, no. 3, p. 213, 2023.

[9] Z. Lei, J. Yang, S. Hao et al., "Purification of quinoline insolubles in heavy coal tar and preparation of mesocarbon microbeads by catalytic polycondensation," *SSRN Electronic Journal*, 2022.

[10] T. D. Dao, H. Lee, and H. M. Jeong, "Alumina-coated graphene nanosheet and its composite of acrylic rubber," *Journal of Colloid and Interface Science*, vol. 416, pp. 38–43, 2014.

[11] M. Kumar, S. Sharma, S. L. Goyal et al., "Composite nanoarchitectonics with reduced-graphene oxide and polyaniline for a highly responsive and selective sensing of methanol vapors," *Materials Chemistry and Physics*, vol. 312, article 128626, 2023.

[12] A. Q. Abdullah, N. A. Ali, S. I. Hussein, A. Hakamy, and A. M. Abd-Elnaiem, "Improving the dielectric, thermal, and electrical properties of poly (methyl methacrylate)/hydroxyapatite blends by incorporating graphene nanoplatelets," *Journal of Inorganic and Organometallic Polymers and Materials*, vol. 33, no. 12, pp. 3882–3893, 2023.

[13] Y. Hua, F. Li, N. Hu, and S. Y. Fu, "Frictional characteristics of graphene oxide-modified continuous glass fiber reinforced epoxy composite," *Composites Science and Technology*, vol. 223, article 109446, 2022.

[14] H. Ramezani, T. Behzad, and R. Bagheri, "Synergistic effect of graphene oxide nanoplatelets and cellulose nanofibers on mechanical, thermal, and barrier properties of thermoplastic starch," *Polymers for Advanced Technologies*, vol. 31, no. 3, pp. 553–565, 2020.

[15] A. Tajdari, A. Babaei, A. Goudarzi, R. Partovi, and A. Rostami, "Hybridization as an efficient strategy for enhancing the performance of polymer nanocomposites," *Polymer Composites*, vol. 42, no. 12, pp. 6801–6815, 2021.

[16] Q. Liu, G. Liu, X. Liu et al., "Synthesis of an electrospun PHA/RGO/Au scaffold for peripheral nerve regeneration: an in vitro study," *Applied Nanoscience*, vol. 10, no. 3, pp. 687–694, 2020.

[17] J. C. Pieretti, T. B. Trevisan, M. M. M. de Moraes, E. A. de Souza, and S. H. Domingues, "High capacitive rGO/WO_3 nanocomposite: the simplest and fastest route of preparing it," *Applied Nanoscience*, vol. 10, no. 1, pp. 165–175, 2020.

[18] B. Sun, W. Chen, H. Zhang et al., "CeO_2-decorated reduced graphene oxide for lubricative, anticorrosive and photocatalytic purposes," *Materials Chemistry and Physics*, vol. 308, p. 128255, 2023.

[19] Z. Huang, P. Luo, S. Jia, H. Zheng, and Z. Lyu, "A sulfur-doped carbon-enhanced $Na_3V_2(PO_4)_3$ nanocomposite for sodium-ion storage," *Journal of Physics and Chemistry of Solids*, vol. 167, article 110746, 2022.

[20] Z. Huang, P. Luo, Q. Wu, and H. Zheng, "Constructing one-dimensional mesoporous carbon nanofibers loaded with $NaTi_2(PO_4)_3$ nanodots as novel anodes for sodium energy storage," *Journal of Physics and Chemistry of Solids*, vol. 161, article 110479, 2022.

[21] A. N. Mohammed Ali, N. A. Ali, S. I. Hussein et al., "Nanoarchitectonics of silver/poly (methyl methacrylate) films: structure, optical characteristics, antibacterial activity, and wettability," *Journal of Inorganic and Organometallic Polymers and Materials*, vol. 33, no. 3, pp. 694–706, 2023.

[22] X. Jia, S. Yu, C. Cheng et al., "Ag nanoparticles modified Fe_3O_4/reduced graphene oxide and their acetone sensing properties," *Materials Chemistry and Physics*, vol. 276, p. 125378, 2022.

[23] Z. Song, D. Han, M. Yang, J. Huang, X. Shao, and H. Li, "Formic acid formation via direct hydration reaction ($CO + H_2O \rightarrow HCOOH$) on magnesia-silver composite," *Applied Surface Science*, vol. 607, article 155067, 2023.

[24] O. Benhabiles, F. Galiano, T. Marino, H. Mahmoudi, H. Lounici, and A. Figoli, "Preparation and characterization of TiO_2-PVDF/PMMA blend membranes using an alternative non-toxic solvent for UF/MF and photocatalytic application," *Molecules*, vol. 24, no. 4, p. 724, 2019.

[25] N. T. Huong, N. M. Dat, D. B. Thinh et al., "Optimization of the antibacterial activity of silver nanoparticles-decorated graphene oxide nanocomposites," *Synthetic Metals*, vol. 268, article 116492, 2020.

[26] X. Zhao, B. Fan, N. Qiao, R. A. Soomro, R. Zhang, and B. Xu, "Stabilized $Ti_3C_2T_x$-doped 3D vesicle polypyrrole coating for efficient protection toward copper in artificial seawater," *Applied Surface Science*, vol. 642, article 158639, 2024.

[27] P. Saxena and P. Shukla, "A comprehensive review on fundamental properties and applications of poly (vinylidene fluoride)(PVDF)," *Advanced Composites and Hybrid Materials*, vol. 4, no. 1, pp. 8–26, 2021.

[28] M. Mohseni and A. Ramazani Saadatabadi, "Highly conductive self-electrical stimuli core-shell conduit based on PVDF-chitosan–gelatin filled with in-situ gellan gum as a possible candidate for nerve regeneration: a rheological, electrical, and structural study," *Applied Nanoscience*, vol. 11, no. 8, pp. 2199–2213, 2021.

[29] R. Jiang, T. Bian, X. Zheng et al., "Corrosion-resistant porous hydrophobic PVDF-CBC foam for the treatment of oil-water separation," *Materials Chemistry and Physics*, vol. 273, p. 125080, 2021.

[30] M. Sharma, K. Sharma, and S. Bose, "Segmental relaxations and crystallization-induced phase separation in PVDF/PMMA blends in the presence of surface-functionalized multiwall carbon nanotubes," *The Journal of Physical Chemistry. B*, vol. 117, no. 28, pp. 8589–8602, 2013.

[31] R. A. Dar, N. G. Khare, D. P. Cole, S. P. Karna, and A. K. Srivastava, "Green synthesis of a silver nanoparticle–graphene oxide composite and its application for As (III) detection," *RSC Advances*, vol. 4, no. 28, pp. 14432–14440, 2014.

[32] D. Wang, Y. Bao, J.-W. Zha, J. Zhao, Z.-M. Dang, and G.-H. Hu, "Improved dielectric properties of nanocomposites based on poly (vinylidene fluoride) and poly (vinyl alcohol)-functionalized graphene," *ACS Applied Materials & Interfaces*, vol. 4, no. 11, pp. 6273–6279, 2012.

[33] N. A. Ali, S. I. Hussein, T. B. Asafa, and A. M. Abd-Elnaiem, "Mechanical properties and electrical conductivity of poly(-methyl methacrylate)/multi-walled carbon nanotubes composites," *Iranian Journal of Science and Technology, Transactions A: Science*, vol. 44, no. 5, pp. 1567–1576, 2020.

[34] M. Sachin, R. Haridass, and B. T. S. Ramanujam, "Polyvinylidene fluoride (PVDF)-poly (methyl methacrylate)(PMMA)-expanded graphite (ExGr) conducting polymer blends: analysis of electrical and thermal behavior," *Materials Today Proceedings*, vol. 28, pp. 103–107, 2020.

[35] R. Sagar, M. S. Gaur, V. Kushwah, A. Rathore, D. G. Piliptsou, and A. A. Rogachev, "Preparation, characterization and microhardness measurements of hybrid nanocomposites based on PMMA+ P (VDF–TrFE) and graphene oxide," *Polymer Bulletin*, vol. 78, no. 12, pp. 7279–7300, 2021.

[36] V. R. Jeedi, E. L. Narsaiah, M. Yalla, R. Swarnalatha, S. N. Reddy, and A. Sadananda Chary, "Structural and electrical studies of PMMA and PVdF based blend polymer electrolyte," *SN Applied Sciences*, vol. 2, no. 12, pp. 1–10, 2020.

[37] I. S. Elashmawi and N. A. Hakeem, "Effect of PMMA addition on characterization and morphology of PVDF," *Polymer Engineering and Science*, vol. 48, no. 5, pp. 895–901, 2008.

[38] X. Zhao, J. Cheng, J. Zhang, S. Chen, and X. Wang, "Crystallization behavior of PVDF/PMMA blends prepared by in situ polymerization from DMF and ethanol," *Journal of Materials Science*, vol. 47, no. 8, pp. 3720–3728, 2012.

[39] A. A. Issa, M. A. Al-Maadeed, A. S. Luyt, D. Ponnamma, and M. K. Hassan, "Physico-mechanical, dielectric, and piezoelectric properties of PVDF electrospun mats containing silver nanoparticles," *C*, vol. 3, no. 4, p. 30, 2017.

[40] D. Uniyal, B. Prasad, K. C. N. Kumar et al., "Impedance characteristics analysis of rGO/polymers (PVDF, PMMA, PTFE) nanocomposite membranes," *Materials Today Proceedings*, vol. 26, pp. 320–323, 2020.

[41] A. Islam, A. N. Khan, M. F. Shakir, and K. Islam, "Strengthening of β polymorph in PVDF/FLG and PVDF/GO nanocomposites," *Materials Research Express*, vol. 7, no. 1, p. 15017, 2019.

[42] J. Yang, Y. Zhang, F. Xue et al., "Structural relaxation and dielectric response of PVDF/PMMA blend in the presence of graphene oxide," *Polymer*, vol. 229, article 123998, 2021.

[43] A. Kausar, H. Ilyas, and M. Siddiq, "Aptitude of graphene oxide–silver in advance polymer nanocomposite: a review," *Polymer - Plastics Technology and Engineering*, vol. 57, no. 4, pp. 283–301, 2018.

[44] D. Liu, W. Li, N. Zhang, T. Huang, J. Yang, and Y. Wang, "Graphite oxide-driven miscibility in PVDF/PMMA blends: assessment through dynamic rheology method," *European Polymer Journal*, vol. 96, pp. 232–247, 2017.

[45] F.-C. Chiu and Y.-J. Chen, "Evaluation of thermal, mechanical, and electrical properties of PVDF/GNP binary and PVDF/PMMA/GNP ternary nanocomposites," *Composites. Part A, Applied Science and Manufacturing*, vol. 68, pp. 62–71, 2015.

[46] K. Sushmita, P. Formanek, D. Fischer, P. Pötschke, G. Madras, and S. Bose, "Ultrathin structures derived from interfacially modified polymeric nanocomposites to curb electromagnetic pollution," *Nanoscale Advances*, vol. 3, no. 9, pp. 2632–2648, 2021.

[47] K. Sushmita, P. Formanek, B. Krause, P. Pötschke, and S. Bose, "Distribution of carbon nanotubes in polycarbonate-based blends for electromagnetic interference shielding," *ACS Applied Nano Materials*, vol. 5, no. 1, pp. 662–677, 2022.

[48] R. Naderi, M. Hajian Heidary, M. Karimi, and A. Ahmadi, "Microstructure and mechanical properties of AA5456/SiO2p nanocomposite fabricated by friction stir processing," *Iranian Journal of Manufacturing Engineering*, vol. 7, no. 4, pp. 39–47, 2020.

[49] R. Moosaei, M. Sharif, and A. Ramezannezhad, "Enhancement of tensile, electrical and thermal properties of epoxy nanocomposites through chemical hybridization of polypyrrole and graphene oxide," *Polymer Testing*, vol. 60, pp. 173–186, 2017.

[50] W. Shao, X. Liu, H. Min, G. Dong, Q. Feng, and S. Zuo, "Preparation, characterization, and antibacterial activity of silver nanoparticle-decorated graphene oxide nanocomposite," *ACS Applied Materials & Interfaces*, vol. 7, no. 12, pp. 6966–6973, 2015.

[51] E. Mahmoudi, L. Y. Ng, W. L. Ang, Y. T. Chung, R. Rohani, and A. W. Mohammad, "Enhancing morphology and separation performance of polyamide 6, 6 membranes by minimal incorporation of silver decorated graphene oxide nanoparticles," *Scientific Reports*, vol. 9, no. 1, pp. 1–16, 2019.

[52] J. Shen, Y. Hu, M. Shi et al., "Fast and facile preparation of graphene oxide and reduced graphene oxide nanoplatelets," *Chemistry of Materials*, vol. 21, no. 15, pp. 3514–3520, 2009.

[53] E. F. Aboelfetoh, A. H. Gemeay, and R. G. El-Sharkawy, "Effective disposal of methylene blue using green immobilized silver nanoparticles on graphene oxide and reduced graphene oxide sheets through one-pot synthesis," *Environmental Monitoring and Assessment*, vol. 192, no. 6, pp. 1–20, 2020.

[54] R. Sharma, A. D. Acharya, S. Moghe et al., "Effect of cobalt doping on microstructural and optical properties of nickel oxide thin films," *Materials Science in Semiconductor Processing*, vol. 23, pp. 42–49, 2014.

[55] S. Stankovich, D. A. Dikin, R. D. Piner et al., "Synthesis of graphene-based nanosheets via chemical reduction of exfoliated graphite oxide," *Carbon*, vol. 45, no. 7, pp. 1558–1565, 2007.

[56] S. Drewniak, R. Muzyka, A. Stolarczyk, T. Pustelny, M. Kotyczka-Morańska, and M. Setkiewicz, "Studies of reduced graphene oxide and graphite oxide in the aspect of their possible application in gas sensors," *Sensors*, vol. 16, no. 1, p. 103, 2016.

[57] X.-Z. Tang, X. Li, Z. Cao et al., "Synthesis of graphene decorated with silver nanoparticles by simultaneous reduction of graphene oxide and silver ions with glucose," *Carbon*, vol. 59, pp. 93–99, 2013.

[58] H. Song, S. Yang, S. Sun, and H. Zhang, "Effect of miscibility and crystallization on the mechanical properties and transparency of PVDF/PMMA blends," *Polymer - Plastics Technology and Engineering*, vol. 52, no. 3, pp. 221–227, 2013.

[59] S. M. Pawde and K. Deshmukh, "Investigation of the structural, thermal, mechanical, and optical properties of poly (methyl methacrylate) and poly (vinylidene fluoride) blends," *Journal of Applied Polymer Science*, vol. 114, no. 4, pp. 2169–2179, 2009.

[60] S. Mohamadi, N. Sharifi-Sanjani, and A. Foyouhi, "Evaluation of graphene nanosheets influence on the physical properties of PVDF/PMMA blend," *Journal of Polymer Research*, vol. 20, no. 1, pp. 1–10, 2013.

[61] E. K. Oikonomou, S. Tencé-Girault, P. Gérard, and S. Norvez, "Swelling of semi-crystalline PVDF by a PMMA-based nanostructured diblock copolymer: morphology and mechanical properties," *Polymer (Guildf).*, vol. 76, pp. 89–97, 2015.

[62] A. Rostami, H. Nazockdast, and M. Karimi, "Graphene induced microstructural changes of PLA/MWCNT biodegradable nanocomposites: rheological, morphological, thermal and electrical properties," *RSC Advances*, vol. 6, no. 55, pp. 49747–49759, 2016.

[63] N. Rajabifar and A. Rostami, "Investigation of the effect of hybrid nanofiller on the mechanical performance and surface properties of bio-based polylactic acid/polyolefin elastomer (PLA/POE) blend," *Polymers*, vol. 15, no. 12, p. 2708, 2023.

[64] A. Rostami and M. I. Moosavi, "High-performance thermoplastic polyurethane nanocomposites induced by hybrid application of functionalized graphene and carbon nanotubes," *Journal of Applied Polymer Science*, vol. 137, no. 14, p. 48520, 2020.

[65] R. K. Layek, S. Samanta, D. P. Chatterjee, and A. K. Nandi, "Physical and mechanical properties of poly (methyl methacrylate)-functionalized graphene/poly (vinylidine fluoride) nanocomposites: piezoelectric β polymorph formation," *Polymer*, vol. 51, no. 24, pp. 5846–5856, 2010.

[66] J. Du and H. Cheng, "The fabrication, properties, and uses of graphene/polymer composites," *Macromolecular Chemistry and Physics*, vol. 213, no. 10-11, pp. 1060–1077, 2012.

[67] S. N. Tripathi, P. Saini, D. Gupta, and V. Choudhary, "Electrical and mechanical properties of PMMA/reduced graphene oxide nanocomposites prepared via in situ polymerization," *Journal of Materials Science*, vol. 48, no. 18, pp. 6223–6232, 2013.

[68] D. Sahu, N. Sarkar, G. Sahoo, P. Mohapatra, and S. K. Swain, "Silver imprinted graphene nanocomposites: synthesisis and morphological study," *Applied Science and Advanced Materials International*, vol. 1, 2015.

[69] A. Soroush, W. Ma, Y. Silvino, and M. S. Rahaman, "Surface modification of thin film composite forward osmosis membrane by silver-decorated graphene-oxide nanosheets," *Environmental Science. Nano*, vol. 2, no. 4, pp. 395–405, 2015.

[70] F. Liu, R. Huo, X. Huang, Q. Lei, and P. Jiang, "Crystalline properties, dielectric response and thermal stability of in-situ reduced graphene oxide/poly (vinylidene fluoride) nanocomposites," *IEEE Transactions on Dielectrics and Electrical Insulation*, vol. 21, no. 4, pp. 1446–1454, 2014.

[71] F. He, S. Lau, H. L. Chan, and J. Fan, "High dielectric permittivity and low percolation threshold in nanocomposites based on poly (vinylidene fluoride) and exfoliated graphite nanoplates," *Advanced Materials*, vol. 21, no. 6, pp. 710–715, 2009.

[72] J. Yu, X. Huang, C. Wu, and P. Jiang, "Permittivity, thermal conductivity and thermal stability of poly (vinylidene fluoride)/graphene nanocomposites," *IEEE Transactions on Dielectrics and Electrical Insulation*, vol. 18, no. 2, pp. 478–484, 2011.

[73] Z. Wang, J. K. Nelson, H. Hillborg, S. Zhao, and L. S. Schadler, "Graphene oxide filled nanocomposite with novel electrical and dielectric properties," *Advanced Materials*, vol. 24, no. 23, pp. 3134–3137, 2012.

[74] S. Yang, Z. Huang, Q. Hu et al., "Proportional optimization model of multiscale spherical BN for enhancing thermal conductivity," *ACS Applied Electronic Materials*, vol. 4, no. 9, pp. 4659–4667, 2022.

[75] A. Khorramshokouh, H. Ramezani, M. Sahami, and M. Sharif, *Silver nanoparticles decorated graphene filled PVDF/PMMA blends with advanced electrical, mechanical, and thermal properties*, Researchsquare, 2022.